

On the interaction between a hurricane, the Gulf Stream and coastal sea level

Tal Ezer

Center for Coastal Physical Oceanography

Old Dominion University

4111 Monarch Way, Norfolk, Virginia, 23508, USA

Phone: (757) 683-5631

Corresponding author: T. Ezer (tezer@odu.edu)

Submitted to Ocean Dynamics: April 9, 2018

Revision submitted: June 5, 2018

2 **Abstract** Tropical storms and hurricanes in the western North Atlantic Ocean can impact the U.S. East
3 Coast in several ways. Direct effects include storm surges, winds, waves and precipitation and indirect
4 effects include changes in ocean dynamics that consequently impact the coast. Hurricane Matthew
5 [October, 2016] was chosen as a case study to demonstrate the interaction between an offshore storm,
6 the Gulf Stream (GS) and coastal sea level. A regional numerical ocean model was used, to conduct
7 sensitivity experiments with different surface forcing, using wind and heat flux data from an operational
8 hurricane-ocean coupled forecast system. An additional experiment used the observed Florida Current
9 (FC) transport during the hurricane as an inflow boundary condition. The experiments show that the
10 hurricane caused a disruption in the GS flow that resulted in large spatial variations in temperatures with
11 cooling of up to ~ 4 °C by surface heat loss, but the interaction of the winds with the GS flow also caused
12 some local warming near fronts and eddies (relative to simulations without a hurricane). A considerable
13 weakening of the FC transport ($\sim 30\%$) has been observed during the hurricane (a reduction of ~ 10 Sv in
14 3 days; $1\text{ Sv} = 10^6 \text{ m}^3\text{s}^{-1}$), so the impact of the FC was explored by the model. Unlike the abrupt and large
15 wind-driven storm surge (up to 2 m water level change within 12 hours in the South Atlantic Bight), the
16 impact of the weakening GS on sea level is smaller but lasted for several days after the hurricane
17 dissipated, as seen in both, the model and altimeter data. These results can explain observations that
18 show minor tidal flooding along long stretches of coasts for several days following passages of
19 hurricanes. Further analysis showed the short-term impact of the hurricane winds on kinetic energy
20 versus the long-term impact of the hurricane-induced mixing on potential energy, whereas several days
21 are needed to reestablish the stratification and rebuild the strength of the GS to its pre-hurricane
22 conditions. Understanding the interaction between storms, the Gulf Stream and coastal sea level can help
23 to improve prediction of sea level rise and coastal flooding.

24

25 **Keywords** Coastal Sea Level, Hurricanes, Flooding, Gulf Stream, Florida Current

26

27 **1 Introduction**

28 The two-way interaction between the ocean and tropical storms or hurricanes is usually centered on the
29 heat exchange between the storm and surface ocean temperatures; this exchange is important for the
30 storm's intensity and for ocean cooling (Bender and Ginis 2000; Shay et al. 2000; Li et al. 2002; Oey et
31 al. 2006, 2007; Yablonski et al. 2015). Storms passing over the ocean can also cause increased mixing
32 and changes in ocean currents, as seen for example during Hurricane Wilma [2005], which affected the
33 flow of the Loop Current in the Gulf of Mexico (Oey et al. 2006). Hurricanes and tropical storms often
34 move across the southwestern North Atlantic, where the dominant current is the Gulf Stream (GS).
35 Several studies thus suggest that storms in this area can cause a temporary (but large) reduction in the
36 GS transport. Evidences of such impact of hurricanes on the GS were reported for example, for
37 Hurricane Bill (2009) (Kourafalou et al. 2016), Hurricane Joaquin [2015] (Ezer and Atkinson 2016; Ezer
38 2018) and Hurricane Mathew [2016] (Ezer et al. 2017). Comparisons of the time when hurricanes and
39 tropical storms passed the southwestern North Atlantic over the last 3 decades with the observed
40 transport of the Florida Current (FC) suggest that these seasonal storms can even influence the seasonal
41 cycle of the FC (Ezer 2018). Note that interactions between Pacific Ocean Typhoons and the Kuroshio
42 Current have also been studied in a similar manner (Wu et al. 2008; Liu and Wei 2015).

43 There are four main mechanisms in which intense storms can impact the GS. First, Atlantic
44 tropical storms spend considerable time south or east of the GS before either turning northwest and
45 making landfall on the U.S. East Coast (e.g., Hurricane Sandy, 2012) or moving back offshore (e.g.,
46 Hurricane Joaquin, 2015, and Hurricane Matthew, 2016). During this time the counterclockwise wind is
47 blowing against the northeastward clockwise flow of the GS and can significantly interrupt the GS flow

48 (Ezer et al. 2017; Ezer 2018). Second, the surface heat loss from the upper ocean (Bender and Ginis
49 2000; Shay et al. 2000) which empower the hurricane can cool down the warm GS and the supply of
50 warm waters into higher latitudes downstream. Third, the intense vertical mixing induced by the strong
51 winds and large waves under the hurricane, can degrade the sharp horizontal thermal gradients across
52 the GS; this pressure gradient is the baroclinic geostrophic part of the GS flow. Fourth, the storm surge
53 can pileup water on the coast (on the onshore side of the GS), reducing the sea surface height difference
54 between the onshore and offshore sides of the GS; this will lead to a reduction in the barotropic
55 geostrophic part of the GS flow. The above mechanisms are not independent of each other and can
56 combine to contribute to the reduction of the GS flow (but potentially also to increase flow at some
57 locations if the wind-driven current is in the GS flow direction). These mechanisms were recently
58 studied by Ezer et al. (2017), analyzing output from a NOAA's operational coupled hurricane-ocean
59 modeling system during Hurricane Matthew. However, the operational forecast system, running in real
60 time during a hurricane, does not allow assessment of various aspects of the air-sea coupled system. For
61 example, it is not clear how much of the sea surface temperature change during the hurricane was due to
62 heat loss or due to mixing. Another limitation of using an operational modeling system was that the
63 ocean model part of the coupled system was a basin-scale ocean model that was not intended to be a
64 storm surge prediction model (though it did a decent job in its coastal sea level simulation; Ezer et al.
65 2017). Therefore, in the present study, the momentum and heat fluxes from the coupled system are used
66 to force a regional coastal ocean model (see domain in Fig. 1), and various sensitivity experiments were
67 performed with different forcing, which was not possible with the real-time forecast system.

68 Another aspect of the study is the potential remote influence of a storm on coastal sea level along
69 the U.S. East Coast through the impact of the storm on the flow and structure of the GS. As reported in
70 recent studies, a weakening in the GS flow is often associated with a decrease in the sea level slope

71 across the GS and elevated coastal sea level on the onshore side of the current (Ezer et al. 2013, Ezer
72 and Atkinson 2014, 2017; Ezer 2015, 2016, Ezer et al. 2017; Goddard et al.,2015; Park and Sweet 2015;
73 Wdowinsky et al. 2016). This relation between variations in the GS and coastal sea level had been
74 suggested long time ago (Blaha 1984), but this connection received more attention in recent years since
75 rising sea levels brought many places over a threshold when even a small anomaly over the predicted
76 tide can now cause minor flooding (Ezer and Atkinson 2014). The GS-coastal sea level connection can
77 be detected on a wide range of scales, from long-term sea level acceleration (Boon 2012; Ezer and
78 Corlett 2012; Sallenger et al. 2012) due to potential slowdown of the Atlantic Meridional Overturning
79 Circulation (AMOC) (McCarthy et al. 2012; Smeed et al. 2013) to short-term daily fluctuations (Ezer
80 2016). The present study focuses on short-term variability associated with the interaction of the GS with
81 a hurricane. Due to sea level rise, many coastal cities such as Norfolk, VA, or Miami, FL, have seen
82 acceleration in minor flooding, so that even a slightly elevated water level due to short-term variations in
83 the GS can now cause unexpected tidal flooding (so called “clear day” or “nuisance” flooding) even
84 when there is no storm nearby (Ezer and Atkinson 2014; Park and Sweet 2015; Wdowinski et al. 2016).
85 The mechanism of this observed short-term sea level-GS correlation was explored by Ezer (2016), who
86 showed the role of fast moving barotropic signals that generate coastal trapped waves. The roles of
87 changing wind patterns and atmospheric pressure in coastal sea level variability are also important
88 (Piecuch and Ponte 2015; Piecuch et al. 2016; Woodworth et al. 2016), but they will not be discussed
89 here.

90 The case study presented here involves Hurricane Matthew which developed in the Caribbean in
91 late September 2016, and then moved northward along the southeastern U.S. coast in October 7-9 (Fig.
92 2), causing significant flood damage due to rain and storm surge on coasts from the South Atlantic Bight
93 (SAB) to the Mid-Atlantic Bight (MAB). This hurricane did not make landfall, but it stayed for several

94 days near the GS, causing as much as 50% temporary reduction in its flow, as evident in various
95 observations and models (Ezer et al. 2017). Therefore, this is a good case study to demonstrate the
96 interaction between a hurricane and ocean currents. The main goal of the study is to investigate under
97 controlled model experiments the various interactions between the hurricane, the GS and coastal sea
98 level, so that better understanding of the mechanisms involved is obtained.

99 The study is organized as follows. First, the data sources and the model setting are described in
100 section 2, then results of the different experiments are presented in section 3, and finally a summary and
101 conclusions are offered in section 4.

102

103 **2 Data and model experiments**

104 Six tide gauge stations, 3 in the SAB and 3 in the MAB, are used here (Fig. 1); hourly water levels were
105 obtained from NOAA (<http://opendap.co-ops.nos.noaa.gov/dods/>). Measurements of the daily FC
106 transport by the cable across the Florida Strait (at $\sim 27^\circ\text{N}$) started in 1982 (Baringer and Larsen 2001;
107 Meinen et al. 2010), and available from NOAA's Atlantic Oceanographic and Meteorological
108 Laboratory web page (www.aoml.noaa.gov/phod/floridacurrent/); here, only the data for October, 2016,
109 were used. Six-hourly output from NOAA's coupled operational Hurricane Weather Research and
110 Forecasting (HWRF) and the Princeton Ocean Model (POM) (Yablonsky et al. 2015; Tallapragada et al.
111 2014) were obtained for the period October 7-12, 2016, when the operational system simulated
112 Hurricane Matthew. The same coupled model for the same period had been recently analyzed (see Ezer
113 et al. 2017, for details). The model domain covers the western North Atlantic Ocean (10°N - 47.5°N ,
114 30°W - 100°W). Here, data for only a smaller sub-region were used (Fig. 1), whereas six-hourly fields of

115 surface heat flux and surface wind stress from the coupled model were used as surface boundary
116 conditions of a regional ocean model.

117 The regional ocean model used here (see domain in Fig. 1) is the same as used recently for
118 coastal sea level studies (see Ezer 2016 and Ezer 2017, for details). The numerical ocean model code is
119 based on the generalized coordinate model of Mellor et al. (2002) with a terrain-following vertical grid
120 and a Mellor-Yamada turbulence scheme. The model topography was obtained from the ETOPO5 data
121 with minimum depth of 10 m. The horizontal grid is cartesian with $1/12^\circ$ resolution (~6-8 km grid size),
122 and the vertical grid is sigma (terrain-following) with 21 layers (higher resolution near the surface). The
123 initial condition is the monthly temperature and salinity data. A spin up of 3 month seems to be
124 sufficient for this small domain to produce a relatively realistic-looking GS (Ezer 2016, 2017). The
125 experiments presented here started after the spin up and represent simulations for October 1-15, 2016; in
126 some experiments (see below) data for Hurricane Matthew was provided as forcing for October 7-12.
127 Note however, that without data assimilation and without much longer realistic forcing (surface and
128 lateral boundary conditions), the simulations cannot represent realistic synoptic fields, thus temperature,
129 salinity and the GS eddies and meanders represent natural variability, not the observed values in space
130 and time at that period. This limitation is not of concern here, since the main purpose of the study is the
131 comparison between different sensitivity experiments, not comparison of the model with observations.
132 The only meaningful model-data comparison is for coastal sea level driven by the hurricane winds (see
133 later). Five sensitivity experiments have been conducted:

- 134 1. Control case (“No Hurricane” experiment)- Surface heat flux and surface wind stress are zero.
135 The only forcing is a fixed imposed boundary transports (see Fig. 1): 30 Sv inflow of the Florida
136 Current (FC), 40 Sv inflow of the Slope Current (SC), 30 Sv inflow of the Sargasso Sea (SS) and
137 100 Sv outflow of the Gulf Stream (GS). Only the total transport (vertically integrated velocity)

138 is specified on the boundary together with standard barotropic radiation boundary conditions.
139 The vertical distribution of the velocity near the open boundaries is calculated by the model from
140 the density field in a 1° buffer zone near the southern and eastern open boundaries.

141 2. Hurricane wind case (“Wind” experiment)- Surface wind stress from the coupled HWRF model
142 is added for October 7-12 (during Hurricane Matthew). The wind is interpolated in space and
143 time from the 6-hourly HWRF output into the ocean model. A smoothed transition is
144 implemented at the beginning and end of the hurricane period. Note that in this case surface heat
145 flux is zero and inflow FC transport is constant as in experiment 1.

146 3. Hurricane heat flux case (“HF” experiment)- Surface heat flux from the 6-hourly coupled HWRF
147 model output is used for October 7-12. In this case, wind remains zero everywhere, so that heat
148 loss during the hurricane can be separated from the wind effects. FC transport is constant as in
149 experiment 1.

150 4. Full hurricane case (“Wind+HF” experiment)- Both wind stress and heat flux from the HWRF
151 output are used for October 7-12. FC transport remains constant as in experiment 1.

152 5. Florida Current case (“FC” experiment)- Same as the control run (no wind and no heat flux),
153 except that the constant inflow of the FC is replaced by the observed FC transport for October 1-
154 15. The change in the inflow at the southern boundary at 27°N is balanced by similar outflow
155 that allows to exit the model on the eastern boundary at 60°W , so volume is generally conserved.
156 This experiment is like the experiments conducted by Ezer (2016), though in the latter study
157 artificial oscillations in the FC transport was imposed, while here observed values are used.

158 Comparisons between experiments 2-4 and experiment 1 will demonstrate the impact of the hurricane
159 wind versus the impact of the hurricane-driven oceanic heat loss, and comparisons between experiments
160 5 and 1 will show the impact of the FC. In the analysis, the impact of each forcing will be defined as the
161 difference between a forced case and the control run. One should keep in mind however, that in the real
162 ocean it is difficult to separate between the hurricane impact on the FC (when it passed very close to the
163 Florida Strait) and the impact of the hurricane on the GS downstream when the hurricane moved north.
164 In the model case, experiment 5 represents only the direct impact of the FC on the model (assuming that
165 the hurricane impacts only the FC, but neglecting the wind impact on the rest of the GS) while
166 experiment 4 represents the impact of the hurricane winds on the downstream GS (neglecting the change
167 in the FC).

168

169 **3 Results**

170 **3.1 The impact of the hurricane and the Florida Current on coastal sea level**

171 Storm surge models require high-resolution ocean models and accurate wind field at high temporal and
172 spatial resolutions (e.g., see the storm surge model of the Chesapeake Bay in Garzon et al. 2017). The
173 evaluation by Ezer et al. (2017) of the HWRF coupled model prediction during Hurricane Matthew
174 shows some skill in the prediction of coastal sea level, though storm surge along the U.S. East Coast was
175 underestimated by ~30-50%. This deficiency was expected, since the ocean model part of the coupled
176 system was intended to provide feedback to the hurricane prediction model but was not intended to be a
177 storm surge model which requires more detailed coastal shoreline and topography (the 6-hourly HWRF
178 output also limits the ability to compare the model with hourly tide gauge data).

179 The storm surge along the coast can be clearly seen in Fig. 3; it is defined as the difference (or
180 anomaly) in sea level between experiment 4 and experiment 1. As the hurricane propagated
181 northeastward along the coast, the onshore winds ahead of the storm piled up water on the coast
182 (positive anomaly in red) while the offshore winds in the back of the storm pushed water away from the
183 coast and sea level dropped (negative anomaly in blue). After day 10 the storm dissipated (no longer a
184 hurricane) and moved offshore. However, after day 12, when the remains of the storm were more than
185 800 km from shore, the impact of the storm can still be seen as a higher than normal coastal sea level
186 along the entire coast, from Florida to New Jersey, with particular high waters in the Chesapeake Bay
187 (Fig. 4a). The fact that sea level north/south of the GS is higher/lower than normal, indicates that the
188 storm caused a reduction in the sea level slope across the GS and thus weakened the currents. Altimeter
189 data of sea surface height anomaly (Fig. 4b) confirm the model results, showing higher than normal
190 water along the northern edge of the GS and along the coast from Florida to New Jersey. Note that sea
191 level anomaly is defined differently for the model (difference between two model runs) and the altimeter
192 data (anomaly relative to a long-term mean, which is not available in the model case); nevertheless, both
193 model and satellite data agree on the main impact after the storm moved away. The results demonstrate
194 the difference between a local short-term storm surge that moves with the storm (Fig. 3) and a longer-
195 term, spatially wide impact due to ocean dynamics after the storm disappeared (Fig. 4).

196 Fig. 5 shows a comparison of results from experiment 4 (Wind+HF) with hourly coastal sea level
197 anomaly data. Note that the anomaly data (observed minus tidal prediction) provided by NOAA still had
198 some tidal-like variations which may be related to resonant created by the hurricane. The range of
199 coastal sea level variation during the storm, ~2 m between maximum storm surge and the water level
200 decline in the wake of the storm, was simulated very well in the SAB (Fernandina, FL, Pulaski, GA, and
201 Charleston, SC). A smaller storm surge of ~0.5-1 m was observed and simulated in the MAB (Duck,

202 NC, Norfolk, VA, and Atlantic City, NJ). The skill of this model with respect to wind-driven coastal sea
203 level is somewhat improved over the HWRF simulations (Ezer et al. 2017), though the same wind field
204 was used. Note that observed water levels ahead of the storm were higher than normal due to previous
205 weather systems (see Fig. 2a in Ezer et al. 2017), but the model only used wind data for October 7-12, so
206 model-data comparisons outside this period are not expected to be very accurate. The observations in
207 Fig. 5 show what looks like a quick recovery of sea level from the storm surge during the short period
208 shown, but longer records (not shown) indicated that water level after the storm was higher than before
209 along most of the SAB and MAB coasts- this can be seen in the altimeter data as well (Fig. 4b).

210 Analyzing various observations, including the FC transport, satellite altimeter data and high-
211 frequency radar data, Ezer et al. (2017) show evidence of significant decline in the GS flow during the
212 passage of Hurricane Matthew (by as much as ~50% from the weeks before the hurricane). The
213 observed FC transport at 27°N reflects part of this hurricane-driven change, so experiment 5 (“FC”) was
214 conducted to see the direct impact of the FC alone on coastal sea level, and the results are shown in Fig.
215 6. In 3 days, between October 8 and October 11, the FC transport weakened by ~30% (from ~30 Sv to
216 ~20 Sv; black heavy line in the bottom of Fig. 6). During these 3 days, water level at the 3 SAB stations
217 rose by ~10 cm as a direct impact of the reduction in sea level slope across the GS. In the MAB (where
218 the GS is farther away from the coast) sea level rose by a smaller amount (~2-5 cm). Note that in the
219 experiments with the same model conducted by Ezer (2016, 2017) the coastal sea level response was
220 similar in magnitude, but more coherent along the coast. However, the previous studies used a FC
221 transport that oscillates at a constant frequency for a long period of time, which apparently allowed the
222 ignition of coastal trapped waves along the coast, including resonant amplification at some critical
223 frequencies (Ezer 2016). In any case, all these experiments indicate that in general every 1 Sv decrease
224 in the FC can cause ~1 cm increase in coastal sea level in the SAB. Observations of sea level in south

225 Florida showed similar relation for long term variations (Park and Sweet 2015). Sea level in the MAB is
 226 also anticorrelated with the GS transport (Ezer 2013, 2015, 2016; Ezer and Atkinson 2017), but the
 227 coastal response is more complex there because of the additional influence from variations in the Slope
 228 Current, shift in the GS path, and influence from GS meanders and eddies (Ezer et al. 2013).

229

230 **3.2 The impact of the hurricane on the Gulf Stream transport**

231 As seen in Fig. 6, the FC transport at 27°N decreased by ~30% within 3 days, and as shown in Ezer et
 232 al. (2017), the GS flow when Hurricane Matthew dissipated may have been weaker by as much as ~50%
 233 from its flow a few weeks before Hurricane Matthew entered the region. The hurricane winds covered
 234 large portion of the model domain (Fig. 2) and thus can temporally affect the ocean circulation. To
 235 evaluate the impact of the hurricane on the circulation, the total stream function, ψ , is calculated from
 236 the vertically averaged velocity field, (U, V) , integrated across the domain, starting from $\psi=0$ on land
 237 (assuming surface elevation is smaller than water depth, $\eta \ll h$).

$$238 \quad \psi(x, y, t) = -\int \int_{x \ y} U(x, y, t) h(x, y) dy \quad \text{or} \quad \psi(x, y, t) = \int \int_{x \ y} V(x, y, t) h(x, y) dx \quad (1a,b)$$

239 where

$$240 \quad U(x, y, t) = \int_z u(x, y, z, t) dz \quad \text{and} \quad V(x, y, t) = \int_z v(x, y, z, t) dz \quad (2a,b)$$

241 so that

$$242 \quad U = -\frac{\partial \psi}{\partial y}, \quad V = \frac{\partial \psi}{\partial x} \quad \text{and} \quad \frac{\partial U}{\partial x} + \frac{\partial V}{\partial y} = 0 \quad (3a,b,c)$$

243 The stream function in experiment 4 is shown for two days, October, 8, 2016, when the hurricane was
244 near the northern coast of Florida (Fig. 7a) and October 10, 2016, when the hurricane moved offshore
245 off Cape Hatteras, North Carolina (Fig. 7b). When the hurricane was located close to the coast around
246 30°N the generation of a clockwise circulation cell around the high value in red (Fig. 7c shows the
247 difference between experiment 4 and experiment 1) could potentially increase the GS transport in the
248 SAB by ~ 5 Sv ($\partial\psi/\partial x > 0$ in Eq. 3b). However, when the hurricane moved offshore around 35°N, an
249 anticlockwise circulation cell around the low value in blue (Fig. 7d) was generated, forcing currents in
250 the direction which potentially can reduce the GS transport by almost ~ 15 Sv. The impact on the
251 circulation due to the FC transport alone (without wind) can be evaluated from the difference between
252 experiment 5 (“FC”) and experiment 1. When the inflow into the model was reduced, the GS transport
253 was reduced by ~ 4 Sv on October 8 (Fig. 7e) and by ~ 10 -15 Sv on October 10 (Fig. 7f). The combined
254 impact of the winds and FC is in general agreement with the transport reduction shown in Ezer et al.
255 (2017). Note that in the real ocean the hurricane affects both, the FC and the GS downstream, but in the
256 model experiments the two factors are separated to better understand the mechanism and pattern behind
257 each impact and this is reflected in the differences between Fig. 7d and Fig. 7f.

258

259 **3.3 The impact of the hurricane on surface temperatures and stratification**

260 The impact of hurricanes on cooling of sea surface temperatures (SST) along the storm’s path has been
261 studied before (Bender and Ginis 2000; Shay et al. 2000; Li et al. 2002; Oey et al. 2006, 2007;
262 Yablonski et al. 2015), but the mechanism may be more complex when the underlying ocean currents
263 involve strong flows such as the GS. Fig. 8 shows the SST and its changes when the hurricane started
264 moving offshore and was located just off Cape Hatteras in October 10, 2016. Note that without long-

265 term simulations with observed heat fluxes and data assimilation of the GS location and eddies the
266 model temperature in Fig. 8a (experiment 4) is not expected to resemble the real SST (and the GS path is
267 probably a little too far north). Therefore, the focus here is on the changes in SST (relative to “No
268 Hurricane” case, experiment 1) that were caused by surface winds (Fig. 8c; experiment 2), surface heat
269 flux (Fig. 8d; experiment 3) and both, winds+heat flux (Fig. 8b; experiment 4). A cooling of $\sim 1\text{-}4^\circ\text{C}$ in
270 SST is seen (Fig. 8b), but with very large spatial variations, including some warming on the onshore side
271 of the GS front. The pattern of SST change for this hurricane is quite extensive and different than the
272 typical cooling pattern seen in the wake of the path of other hurricanes (see for example, Fig. 3 in
273 Bender and Ginis 2000, or Fig. 7 in Oey et al. 2007). The experiment with wind only (Fig. 8c) shows
274 that these spatial variations are the result of the interaction of the wind with the GS- impact includes,
275 cooling along the warm core of the GS and (relative) warming of the onshore side of the GS and near the
276 cold-core ring around 70°W , 38°N . In addition to the mixing effect of the wind, a slight northward
277 shift of the GS front in the MAB (relative to the “no hurricane” case) can also cause this relative
278 warming of the onshore side of the GS. The experiment with heat flux only (Fig. 8d) indicates a cooling
279 trend everywhere, but especially large cooling on the shelf and the onshore side of the GS. It is expected
280 that larger SST cooling will occur in regions with shallow continental shelves and shallow mixed layers,
281 as documented in other studies (e.g., Oey et al. 2006, 2007).

282 To further look at the vertical extension of the impact, east-west cross sections of temperature
283 across 38°N are shown in Fig. 9 (same experiments as in Fig. 8). The sea surface height (SSH) and
284 stratification along this section (Fig. 9a) indicates that the section crosses the GS at $\sim 73^\circ\text{W}$ and crosses a
285 cold-core ring at $\sim 70\text{-}71^\circ\text{W}$. As shown in Fig. 8c, most of the spatial variations were due to the impact
286 of the wind (Fig. 9c), which caused cooling of the continental shelf by upwelling and cooling of the
287 upper ~ 50 m by vertical mixing. However, winds can also cause warming near the GS front and near the

288 cold-core ring (mixing of the cold ring with surrounded warmer waters may have caused this). The
 289 impact of heat flux is more spatially even with a cooling trend everywhere above ~30 m (Fig. 8d). As
 290 shown by Oey et al. (2006), hurricanes can generate internal waves and very strong vertical velocities in
 291 their wake which may explain some of the variations in Fig. 9c. However, a more detailed study of these
 292 convective processes and breaking of internal waves will require the usage of non-hydrostatic models
 293 (e.g., Legg and Adcroft 2003), which is beyond the scope of this study.

294

295 **3.4 The impact of the hurricane on kinetic and potential energy**

296 To see how the hurricane impacted the upper ocean flow and the upper ocean stratification, the changes
 297 in mean kinetic energy and mean potential energy during the hurricane are estimated. The mean kinetic
 298 energy per unit mass of the upper 50 m averaged over the entire model domain is defined by

$$299 \quad KE(t) = \frac{0.5}{VOL} \int \int \int_{x,y,z=-50m}^0 [u(x,y,z,t)^2 + v(x,y,z,t)^2] dx dy dz, \quad VOL = \int \int \int_{x,y,z=-50m}^0 dx dy dz \quad (4)$$

300 and the relative mean potential energy change per unit mass is defined here by

$$301 \quad PE(t) = \frac{g}{VOL} \int \int \int_{x,y,z=-50m}^0 z \left[\frac{\rho(x,y,z,t) - \rho_0(x,y,z)}{\rho_0(x,y,z)} \right] dx dy dz \quad (5)$$

302 where the reference density ρ_0 is the initial condition prior to the hurricane. In (5), cooling and increased
 303 density would result in more negative PE ($z < 0$), i.e., less energy is needed to mix the water column. One
 304 should not expect a balance between KE and PE in the upper 50 m, as input of wind energy involves
 305 momentum and heat exchange with deeper layers and the generation of eddy kinetic energy. The main
 306 purpose of these calculations is to evaluate the impact of the hurricane on the flow (4) and stratification

307 (5). Therefore, the changes in upper ocean KE and PE are calculated as the difference of each case with
308 the “no hurricane” (experiment 1), and the results are shown in Fig. 10. The maximum KE due to the
309 hurricane winds (Fig. 10a) occurred on October 7. Note the slightly larger KE for “WIND only”
310 (experiment 2) case compared with “WIND+HF” (experiment 4); the additional cooling in the
311 WIND+HF case increases the density of the upper layers, thus reducing velocities since more energy is
312 needed to move a layer with a larger mass. As expected, the impact of “HF” (experiment 3) or “FC”
313 (experiment 5) alone on KE is much smaller than the wind impact. The reduction of the FC transport in
314 the latter experiment seems to affect mostly the total transport (Fig. 7f) and much less so for the mean
315 surface flow, except near the GS itself.

316 The change in PE is somewhat less expected, especially the “WIND” only case (green line in
317 Fig. 10b) that indicates relative net warming of the upper layers despite the induced mixing. All the
318 other cases indicate net cooling of the upper layers which increases density there and resulted in more
319 negative PE. In the “WIND” only case, in addition to local warming spots near the GS front, most of the
320 southeastern part of the model domain has warmed by advection of warm waters from the south (Fig.
321 8c). This slight warming is explained by the fact that most of the model domain was under the influence
322 of the northward winds east of the eye of the storm. The largest reduction in PE is for the “WIND+HF”
323 case which induced more cooling than the separate impacts of “WIND” + “HF”. This result indicates the
324 non-linear nature of the surface forcing where the maximum impact is obtained when wind-induced
325 mixing is combined with surface heat loss. The impact of FC alone is a very small reduction in PE when
326 the transport of the FC is reduced and the rate of warm waters advected from the Florida Strait
327 downstream is reduced. One of the important conclusions from Fig. 10, is the difference in timing
328 between the immediate KE increase by the hurricane winds (peak KE on October 7) and the delay
329 response of PE that seems to last for days after the hurricane had dissipated. The disruption to the GS

330 flow and erosion of the stratification can keep the GS in a state of weaker than normal flow (and
331 elevated coastal water levels, as discussed before) for days after the hurricane disappeared. One can
332 estimate how long it would take for the GS to completely recover by only advection of new warm waters
333 from the Florida Strait downstream (neglecting wind and heat fluxes). At velocity speed of $\sim 1 \text{ m s}^{-1}$ it
334 would take warm waters from the Florida Strait almost a month to reach the northeastern part of the GS
335 ($\sim 2500 \text{ km}$ away). This can explain the unpredictable minor tidal flooding that are often observed
336 following remote storms far away from the flooding area (Ezer and Atkinson 2014, 2016, Ezer et al.
337 2017).

338

339 **4. Summary and conclusions**

340 The interconnections between variations in the GS flow, variations in coastal sea level and Atlantic
341 Ocean variability over wide range of time scales have been an area of intense research in recent years.
342 The long-term implications are related for example, to climate change and sea level rise acceleration due
343 to potential GS slowdown (Sallenger et al. 2012; Ezer et al. 2013) while short-term variability is related
344 for example, to increase in the frequency of minor tidal flooding (Ezer and Atkinson 2014), or the
345 indirect effect of a hurricane on ocean dynamics (Ezer et al. 2017; Ezer, 2018). Recent “clear-day”
346 floods in coastal cities such as Norfolk, VA, often last several days after hurricanes passed off the
347 Florida coast, even though the hurricanes remained thousands of kilometers away and never made
348 landfall; examples are Hurricane Joaquin [2015] and Hurricane Matthew [2016]. A recent study of
349 Hurricane Matthew (Ezer et al. 2017), used various observations and output from a coupled ocean-
350 atmosphere operational forecast system to describe the disruption that the hurricane caused to the GS
351 flow, which temporally weakened the GS and contributed to elevated coastal sea level (in addition to the

352 storm surge). Following the above study, sensitivity experiments with a regional ocean model are
353 conducted here to better understand the interplay between the hurricane, the GS and coastal sea level,
354 using data from Hurricane Matthew.

355 The results demonstrate the distinctly different impact of surface heat loss versus surface wind
356 stress versus the impact of the FC by comparing simulations with different forcing with simulations of
357 the GS without the hurricane. Because of the passage of that hurricane near the strong currents of the
358 GS, the pattern of SST change had much more spatial variations than usually seen in the wake of a
359 hurricane (e.g., see Bender and Ginis 2000). The wind mixing and its interaction with the GS caused
360 spatial changes to upper ocean temperatures near the GS front and near eddies (with local warming at
361 some locations) while surface heat loss caused a more even cooling that is enhanced in shallow regions.
362 The coastal sea level response to wind-driven storm surge is large near the storm, but that anomaly lasts
363 for only a short period of few hours, while the response to disruption to the GS or related weakening of
364 the FC seemed to last for days after the hurricane disappeared. Analysis of kinetic and potential energy
365 confirms that it takes a long time for the stratification to recover after a hurricane- a week after the peak
366 of the hurricane-induced kinetic energy, the potential energy remained low. This result can explain the
367 observations that show elevated water levels and minor tidal flooding for days following a hurricane.
368 Better understanding of these remote influences on coastal sea level can help to improve prediction
369 models, which rely mostly on local wind, but have difficulty in accounting for indirect remote influence
370 associated with ocean dynamics.

371

372 **Acknowledgments** Old Dominion University's Climate Change and Sea Level Rise Initiative
373 (CCSLRI) and the Resilience Collaborative (ODU-RC) provided partial support for this study and the

374 Center for Coastal Physical Oceanography (CCPO) provided computational support. The hourly tide
375 gauges sea level data are available from: (<http://opendap.co-ops.nos.noaa.gov/dods/>). The Florida
376 Current transport record is obtained from: <http://www.aoml.noaa.gov/phod/floridacurrent/>. The HWRF
377 model results are available from NOAA/NCEP (http://www.emc.ncep.noaa.gov/gc_wmb/vxt/HWRF/).

378

379 **References**

380 Baringer MO, Larsen JC (2001) Sixteen Years of Florida Current Transport at 27°N. *Geophys Res Lett*
381 28(16):3,179-3,182. <https://doi.org/10.1029/2001GL013246>

382 Bender MA, Ginis I (2000) Real-case simulations of hurricane–ocean interaction using a high-resolution
383 coupled model: effects on hurricane intensity. *Mon. Wea. Rev.* 128:917–946.
384 [https://doi.org/10.1175/1520-0493\(2000\)128<0917:RCSOHO>2.0.CO;2](https://doi.org/10.1175/1520-0493(2000)128<0917:RCSOHO>2.0.CO;2)

385 Blaha JP (1984) Fluctuations of monthly sea level as related to the intensity of the Gulf Stream from
386 Key West to Norfolk. *J Geophys Res Oceans* 89(C5):8033-8042.
387 <https://doi.org/10.1029/JC089iC05p08033>

388 Boon JD (2012) Evidence of sea level acceleration at U.S. and Canadian tide stations, Atlantic coast,
389 North America. *J Coast Res* 28(6):1437–1445. <https://doi.org/10.2112/JCOASTRES-D-12-00102.1>

390 Ezer T (2013) Sea level rise, spatially uneven and temporally unsteady: Why the U.S. East Coast, the
391 global tide gauge record, and the global altimeter data show different trends. *Geophys Res Lett*
392 40:5439–5444. <https://doi.org/10.1002/2013GL057952>

393 Ezer T (2015) Detecting changes in the transport of the Gulf Stream and the Atlantic overturning
394 circulation from coastal sea level data: The extreme decline in 2009-2010 and estimated variations
395 for 1935-2012. *Glob Planet Change* 129:23-36. <https://doi.org/10.1016/j.gloplacha.2015.03.002>

396 Ezer T (2016) Can the Gulf Stream induce coherent short-term fluctuations in sea level along the U.S.
397 East Coast?: A modeling study. *Ocean Dyn* 66(2):207-220. [https://doi.org/10.1007/s10236-016-0928-](https://doi.org/10.1007/s10236-016-0928-0)
398 0

399 Ezer T (2017) A modeling study of the role that bottom topography plays in Gulf Stream dynamics and
400 in influencing the tilt of mean sea level along the U.S. East Coast, *Ocean Dynamics*, 67(5), 651-664,
401 doi:10.1007/s10236-017-1052-5.

402 Ezer, T (2018) The increased risk of flooding in Hampton Roads: On the roles of sea level rise, storm
403 surges, hurricanes and the Gulf Stream. In: *The Hampton Roads Sea Level Rise Preparedness and*
404 *Resilience Intergovernmental Pilot Project*, Toll, R. and G. F. Kuska (Eds.). *Mar Tech Soc J*
405 52(2):34-44. <https://doi.org/10.4031/MTSJ.52.2.6>

406 Ezer T, Corlett WB (2012) Is sea level rise accelerating in the Chesapeake Bay? A demonstration of a
407 novel new approach for analyzing sea level data. *Geophys Res Lett* 39:L19605.
408 <https://doi.org/10.1029/2012GL053435>

409 Ezer T, Atkinson LP (2014) Accelerated flooding along the U.S. East Coast: On the impact of sea-level
410 rise, tides, storms, the Gulf Stream, and the North Atlantic Oscillations. *Earth's Future* 2(8):362-382.
411 <https://doi.org/10.1002/2014EF000252>

412 Ezer T, Atkinson LP (2017) On the predictability of high water level along the U.S. East Coast: can the
413 Florida Current measurement be an indicator for flooding caused by remote forcing?, *Ocean Dyn*
414 67(6):751-766. <https://doi.org/10.1007/s10236-017-1057-0>

415 Ezer T, Atkinson LP, Corlett WB, Blanco JL (2013) Gulf Stream's induced sea level rise and variability
416 along the U.S. mid-Atlantic coast. *J Geophys Res Oceans* 118:685–697.
417 <https://doi.org/10.1002/jgrc.20091>

418 Ezer T, Atkinson LP, Tuleya R (2017) Observations and operational model simulations reveal the
419 impact of Hurricane Matthew (2016) on the Gulf Stream and coastal sea level. *Dyn Atmos Oceans*
420 80:124-138. <https://doi.org/10.1016/j.dynatmoce.2017.10.006>

421 Garzon JL, Ferreira CM, Padilla-Hernandez R (2017) Evaluation of weather forecast system for storm
422 surge modeling in the Chesapeake Bay. *Ocean Dyn* 68(1):91-107. [https://doi.org/10.1007/s10236-](https://doi.org/10.1007/s10236-017-1120-x)
423 017-1120-x

424 Goddard PB, Yin J, Griffies SM, Zhang S (2015) An extreme event of sea-level rise along the Northeast
425 coast of North America in 2009–2010. *Nature Comm* 6:6345. <https://doi.org/10.1038/ncomms7346>

426 Kourafalou VH, Androulidakis YS, Halliwell GR, Kang HS, Mehari MM, Le Hénaff M, Atlas R,
427 Lumpkin R (2016) North Atlantic Ocean OSSE system development: Nature Run evaluation and
428 application to hurricane interaction with the Gulf Stream. *Prog Oceanogr* 148:1–25.
429 <https://doi.org/10.1016/j.pocean.2016.09.001>

430 Legg S, Adcroft A (2003) Internal wave breaking at concave and convex continental slopes. *J Phys*
431 *Oceanogr* 33(11):2224-2246. [https://doi.org/10.1175/1520-](https://doi.org/10.1175/1520-0485(2003)033<2224:IWBACA>2.0.CO;2)
432 0485(2003)033<2224:IWBACA>2.0.CO;2

433 Li Y, Xue H, Bane JM (2002) Air-sea interactions during the passage of a winter storm over the Gulf
434 Stream: A three-dimensional coupled atmosphere-ocean model study. *J Geophys Res Oceans*
435 107(C11). <https://doi.org/10.1029/2001JC001161>

436 Liu X, Wei J (2015) Understanding surface and subsurface temperature changes induced by tropical
437 cyclones in the Kuroshio. *Ocean Dyn.* 65(7):1017-1027. <https://doi.org/10.1007/s10236-015-0851-9>

438 McCarthy G, Frejka-Williams E, Johns WE, Baringer MO, Meinen CS, Bryden HL, Rayner D, Duchez
439 A, Roberts C, Cunningham SA (2012) Observed interannual variability of the Atlantic meridional
440 overturning circulation at 26.5°N. *Geophys Res Lett* 39(19):L19609.
441 <https://doi.org/10.1029/2012GL052933>

442 Meinen CS, Baringer MO, Garcia RF (2010) Florida Current transport variability: An analysis of annual
443 and longer-period signals. *Deep Sea Res* 57(7):835–846. <https://doi.org/10.1016/j.dsr.2010.04.001>

444 Oey LY, Ezer T, Wang DP, Fan SJ, Yin XQ (2006) Loop Current warming by Hurricane Wilma.
445 *Geophys Res Lett* 33:L08613. <https://doi.org/10.1029/2006GL025873>

446 Oey LY, Ezer T, Wang DP, Yin XQ, Fan SJ (2007) Hurricane-induced motions and interaction with
447 ocean currents. *Cont Shelf Res* 27:1249-1263. <https://doi.org/10.1016/j.csr.2007.01.008>

448 Park J, Sweet W (2015) Accelerated sea level rise and Florida current transport. *Ocean Sci.*, 11:607–
449 615. <https://doi.org/10.5194/os-11-607-2015>

450 Piecuch CG, Ponte RM (2015) Inverted barometer contributions to recent sea level changes along the
451 northeast coast of North America. *Geophys Res Lett* 42:5918–5925.
452 <https://doi.org/10.1002/2015GL064580>

453 Piecuch CG, Dangendorf S, Ponte R, Marcos M (2016) Annual sea level changes on the North
454 American Northeast Coast: influence of local winds and barotropic motions. *J Clim* 29:4801–4816.
455 <https://doi.org/10.1175/JCLI-D-16-0048.1>

456 Sallenger AH, Doran KS, Howd P (2012) Hotspot of accelerated sea-level rise on the Atlantic coast of
457 North America. *Nat Clim Change* 2:884-888. <https://doi.org/10.1038/NCILMATE1597>

458 Shay LK, Goni GJ, Black PG (2000) Effects of a warm oceanic feature on hurricane Opal. *Mon Wea*
459 *Rev* 128:1366–1383. [https://doi.org/10.1175/1520-0493\(2000\)128<1366:EOAWOF>2.0.CO;2](https://doi.org/10.1175/1520-0493(2000)128<1366:EOAWOF>2.0.CO;2)

460 Smeed DA, McCarthy G, Cunningham SA, Frajka-Williams E, Rayner D, Johns WE, Meinen CS,
461 Baringer MO, Moat BI, Duchez A, Bryden HL (2013) Observed decline of the Atlantic Meridional
462 Overturning Circulation 2004 to 2012. *Ocean Sci Discuss* 10:1619-1645. [https://doi.org/10.5194/osd-](https://doi.org/10.5194/osd-10-1619-2013)
463 [10-1619-2013](https://doi.org/10.5194/osd-10-1619-2013)

464 Tallapragada V, Bernardet L, Biswas MK, Gopalakrishnan S, Kwon Y, Liu Q, Marchok T, Sheinin D,
465 Tong M, Trahan S, Tuleya R, Yablonsky R, Zhang X (2014) Hurricane Weather Research and
466 Forecasting (HWRF) Model: 2014 Scientific Documentation. Editor: L. Bernardet. NCAR
467 Development Tested Bed Center Report, 81pp, Boulder, CO.

468 Wdowinski S, Bray R, Kirtman BP, Wu Z (2016) Increasing flooding hazard in coastal communities due
469 to rising sea level: Case study of Miami Beach, Florida. *Ocean Coast Man* 126:1–8.
470 <https://doi.org/10.1016/j.ocecoaman.2016.03.002>

471 Woodworth PL, Maqueda MM, Gehrels WR, Roussenov VM, Williams RG, Hughes CW (2016)
472 Variations in the difference between mean sea level measured either side of Cape Hatteras and their

473 relation to the North Atlantic Oscillation. *Clim Dyn* 49(7-8):2451-2469.
474 <https://doi.org/10.1007/s00382-016-3464-1>

475 Wu CR, Chang YL, Oey LY, Chang CWJ, Hsin YC (2008) Air-sea interaction between tropical cyclone
476 Nari and Kuroshio. *Geophys Res Lett* 31:L12605. <https://doi.org/10.1029/2008GL033942>

477 Yablonsky RM, Ginis I, Thomas B, Tallapragada V, Sheinin D, Bernardet L (2015) Description and
478 analysis of the ocean component of NOAA's operational Hurricane Weather Research and
479 Forecasting (HWRF) Model. *J Atmos Ocean Tech* 32:144-163. [https://doi.org/10.1175/JTECH-D-14-](https://doi.org/10.1175/JTECH-D-14-00063.1)
480 00063.1

481

482

483 **Figure Captions:**

484

485 **Fig. 1.** Bottom topography (color in meter) of the region and model domain (dashed line). Six tide gauge
486 stations used in the study are indicated (diamonds with numbers). The location of imposed model's
487 inflows (Florida Current, FC; Slope Current, SC and Sargasso Sea, SS) and outflow (Gulf Stream, GS)
488 are indicated (wide arrows), as well as schematic of the main currents (narrow arrows).

489

490 **Fig. 2.** The maximum wind field (color in knots) from the operational forecast of the HWRF-POM
491 model for Hurricane Matthew (October 7-12, 2016) and storm predicted track ("x" and blue line). The
492 figure is a modified version of the one on the NOAA site

493 (http://www.emc.ncep.noaa.gov/gc_wmb/vxt/HWRF/).

494

495 **Fig. 3.** The model storm surge (color in m) defined as the sea level difference (anomaly) between
496 experiment 4 (WIND+HF) and experiment 1 (NO-HURRICANE); panels (a)-(d) are for days 8-9.5. The
497 heavy black contours indicate the estimated extent of the strong winds (outer/inner lines are for wind
498 speed $> 25/35$ m s⁻², respectively). The gray lines show a few contours of the absolute sea surface height
499 in experiment 4, to indicate the location of the Gulf stream.

500

501 **Fig. 4.** (a) The model sea level anomaly as in Fig. 3, but for day 12 after the storm moved away from the
502 coast (note that the color scale is different than that of Fig. 3). (b) Sea level anomaly from satellite
503 altimeters (from AVISO) on October 12, 2016; the approximated location of the Gulf Stream is
504 indicated by a dashed white line. Note that the domains and the color bars of (a) and (b) are different,

505 and that sea level anomaly is defined differently: in (a) the anomaly is the difference between two model
506 simulations for the same day, while in (b) the anomaly is the observed sea surface height at that day
507 relative to a long-term mean of absolute sea surface height.

508

509 **Fig. 5.** Hourly water level anomalies at the six locations in Fig. 1 (relative values in m were vertically
510 shifted for clarity) as obtained from the tide gauges (green circles; predicted tides were subtracted) and
511 from the model forced by hurricane winds (experiment 4; black lines). Hurricane winds were applied in
512 the model only during October 7-12 (dashed horizontal line).

513

514 **Fig. 6.** Hourly simulated water levels (in cm, blue lines, shifted vertically for clarity) at the same
515 locations as in Fig. 5, but without wind (experiment 5) when the only forcing of the model is the
516 observed daily Florida Current transport (in Sv, black line at the bottom).

517

518 **Fig. 7.** Model stream function in Sv for (a) October 8 and (b) October 10, and the change at those dates
519 due to the hurricane wind (c and d) and due to the FC (e and f). The change in transport is the difference
520 between the simulation with and without hurricane (c and d; experiment 4 minus experiment 1) or with
521 and without time-dependent FC (e and f; experiment 5 minus experiment 1). Note the different color bar
522 scale in each panel, contour interval is 5 Sv in (a)-(b) and 1 Sv in (c)-(f). The estimated location of the
523 hurricane eye is indicated in c and d.

524

525 **Fig. 8.** (a) Model Sea Surface Temperature (SST) on October 10 (experiment 4) and the impact of (b)
526 WIND+HF (experiment 4 minus experiment 1), (c) WIND only (experiment 2 minus experiment 1) and
527 (d) HF only (experiment 3 minus experiment 1).

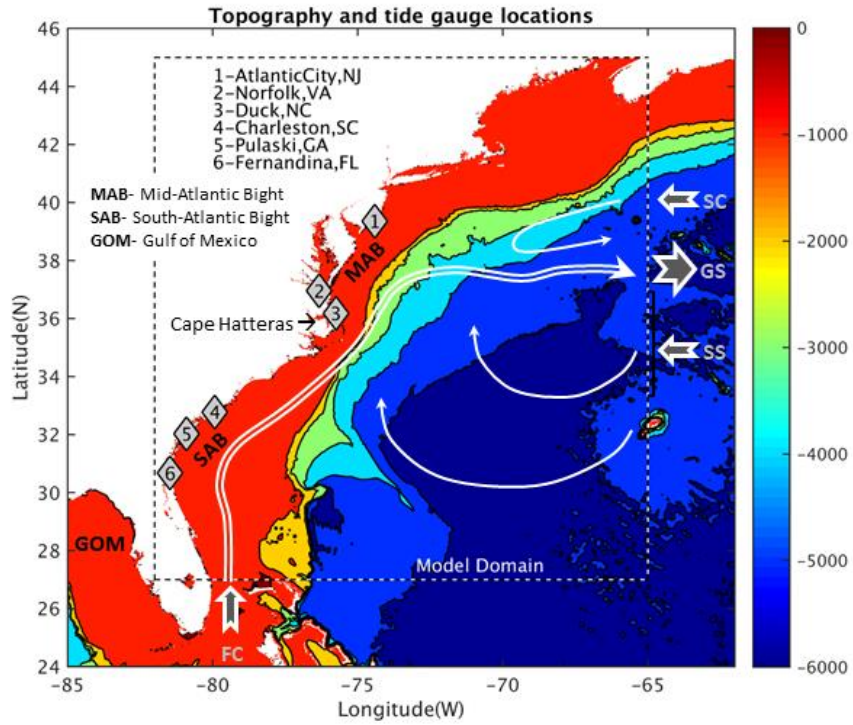
528

529 **Fig. 9.** East-west cross section at 38°N on October 10, 2016. (a) Temperature for hurricane case
530 (experiment 4, WIND+HF), (b) temperature change due to the hurricane (experiment 4 minus
531 experiment 1), (c) temperature change due to the WIND only (experiment 2 minus experiment 1) and (d)
532 temperature change due to the HF only (experiment 3 minus experiment 1). Note that (b)-(d) only show
533 the upper 100 m and the color bar is different than in (a). Contour interval is 2°C in (a) and black
534 contour in (b)-(d) is the zero line.

535

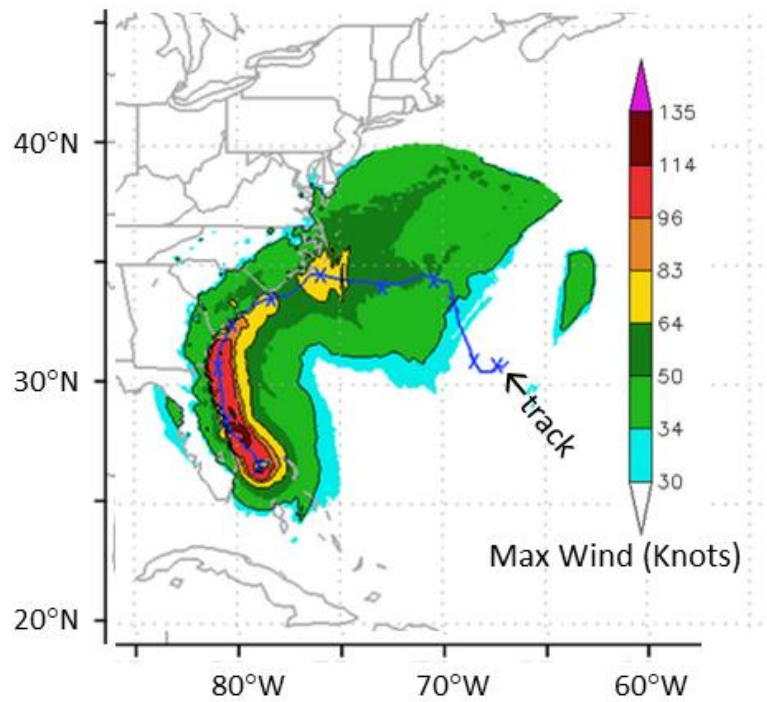
536 **Fig. 10.** Daily changes in the average (a) kinetic energy and (b) potential energy for the different
537 experiments (in different color lines as indicated). The changes are the anomalies relative to the control
538 run (no hurricane case). The values are energy per unit mass averaged over the upper 50 m of the entire
539 model domain.

540

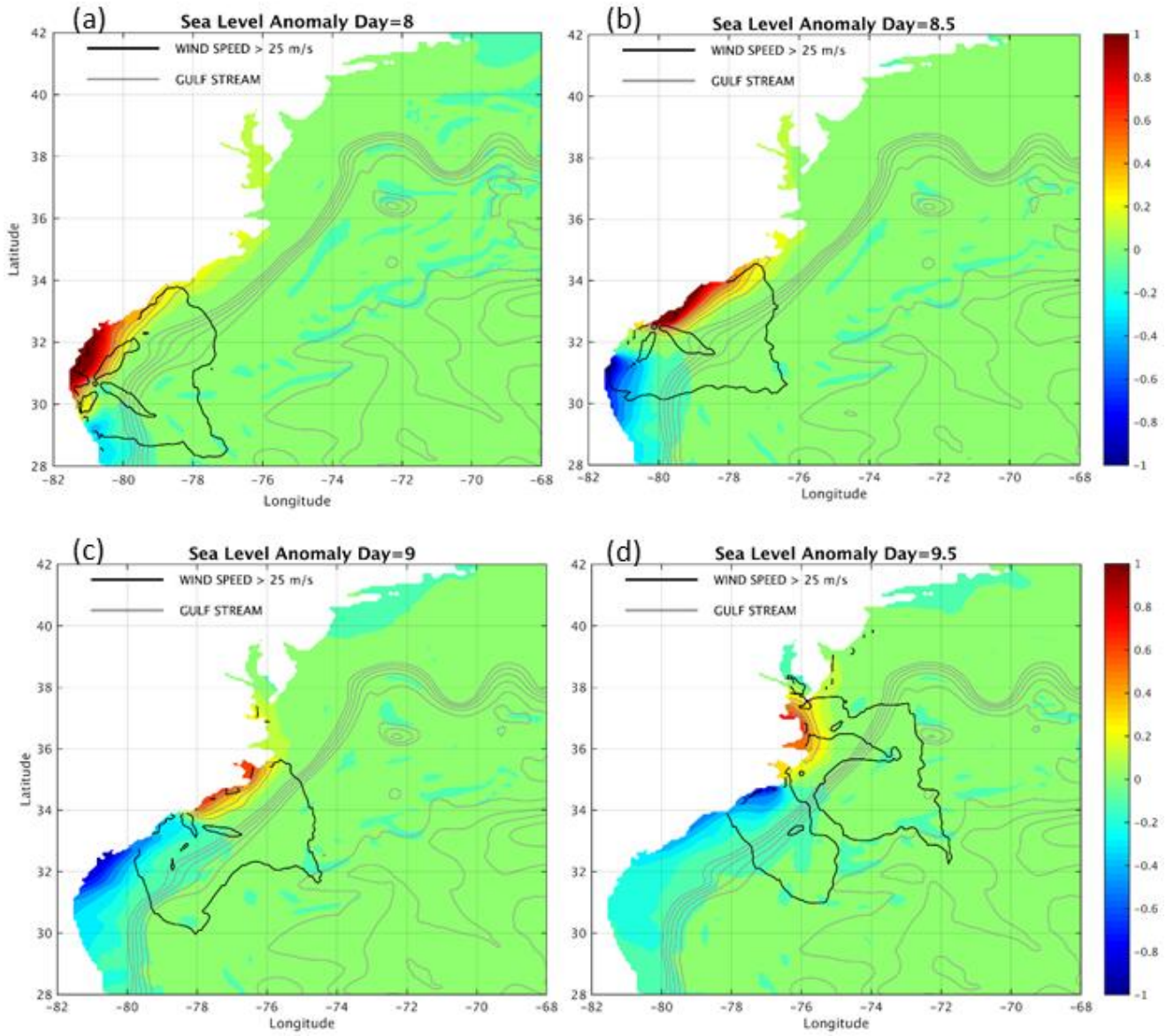


541
 542 Fig. 1
 543

HWRF Forecast of Hurricane Matthew Oct 7-12, 2016

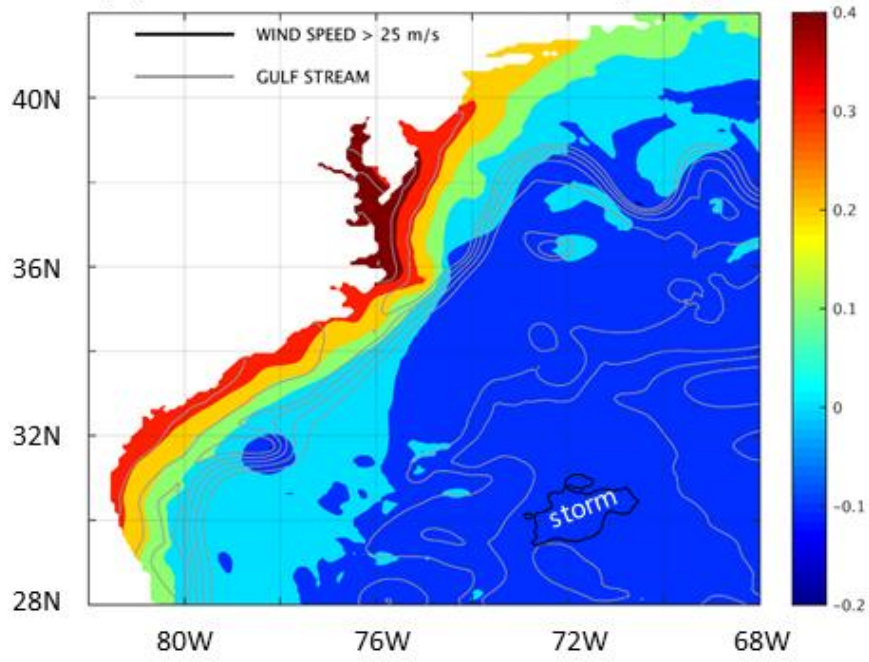


544
 545 Fig. 2
 546

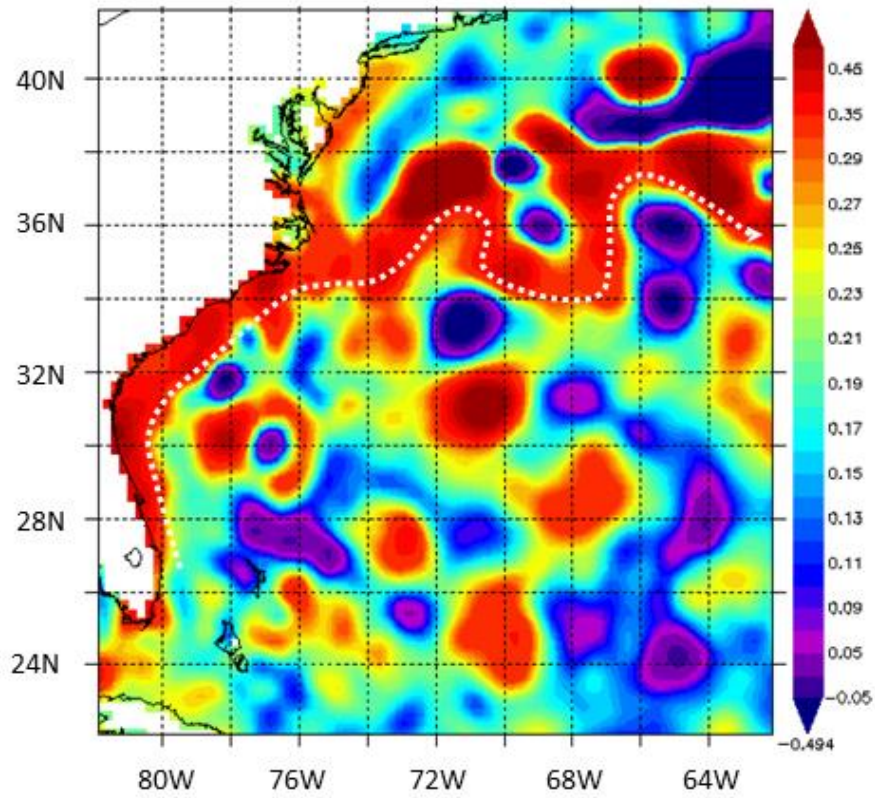


547
 548 Fig. 3
 549

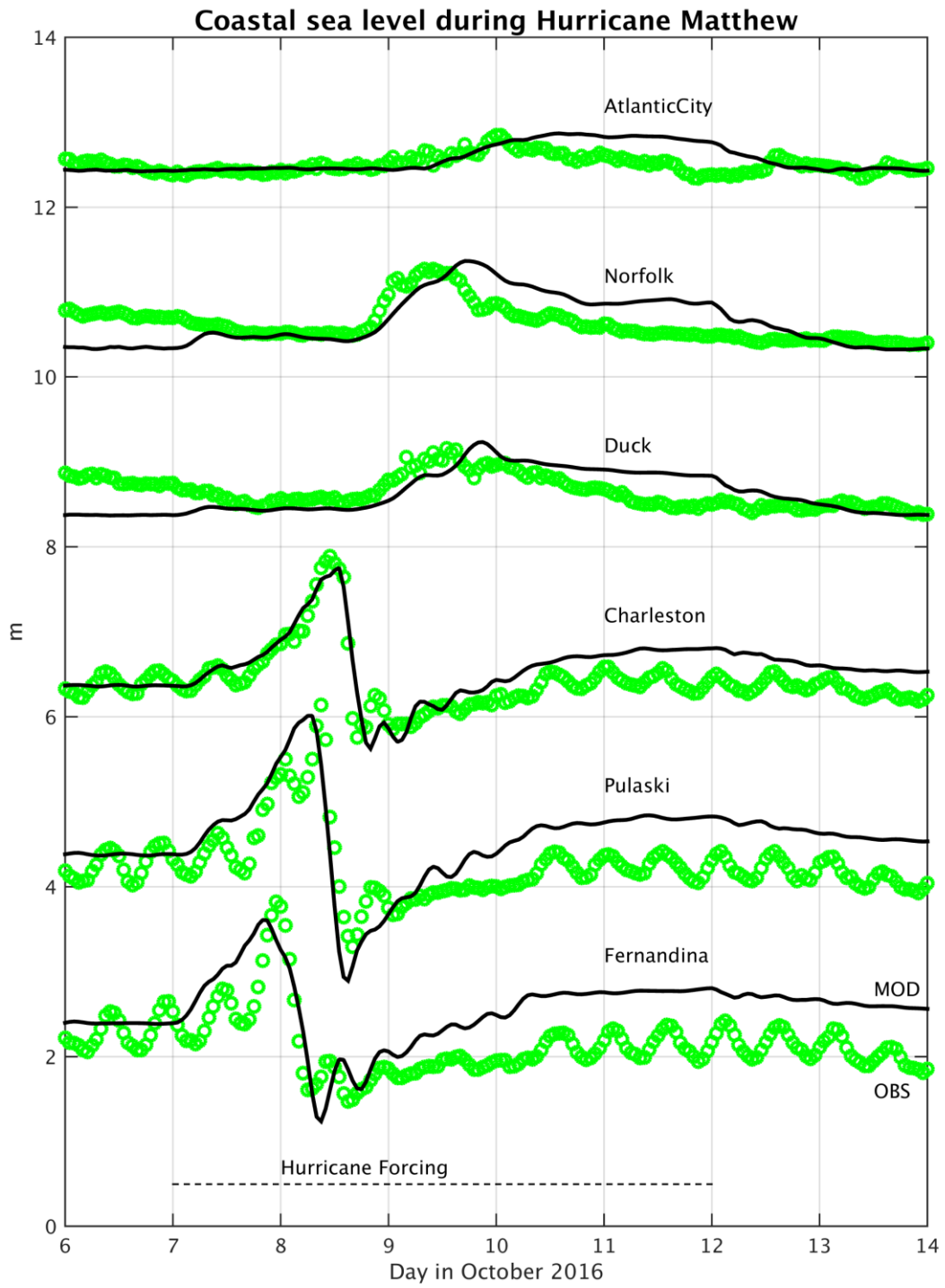
(a) Model Sea Level Anomaly Day=12



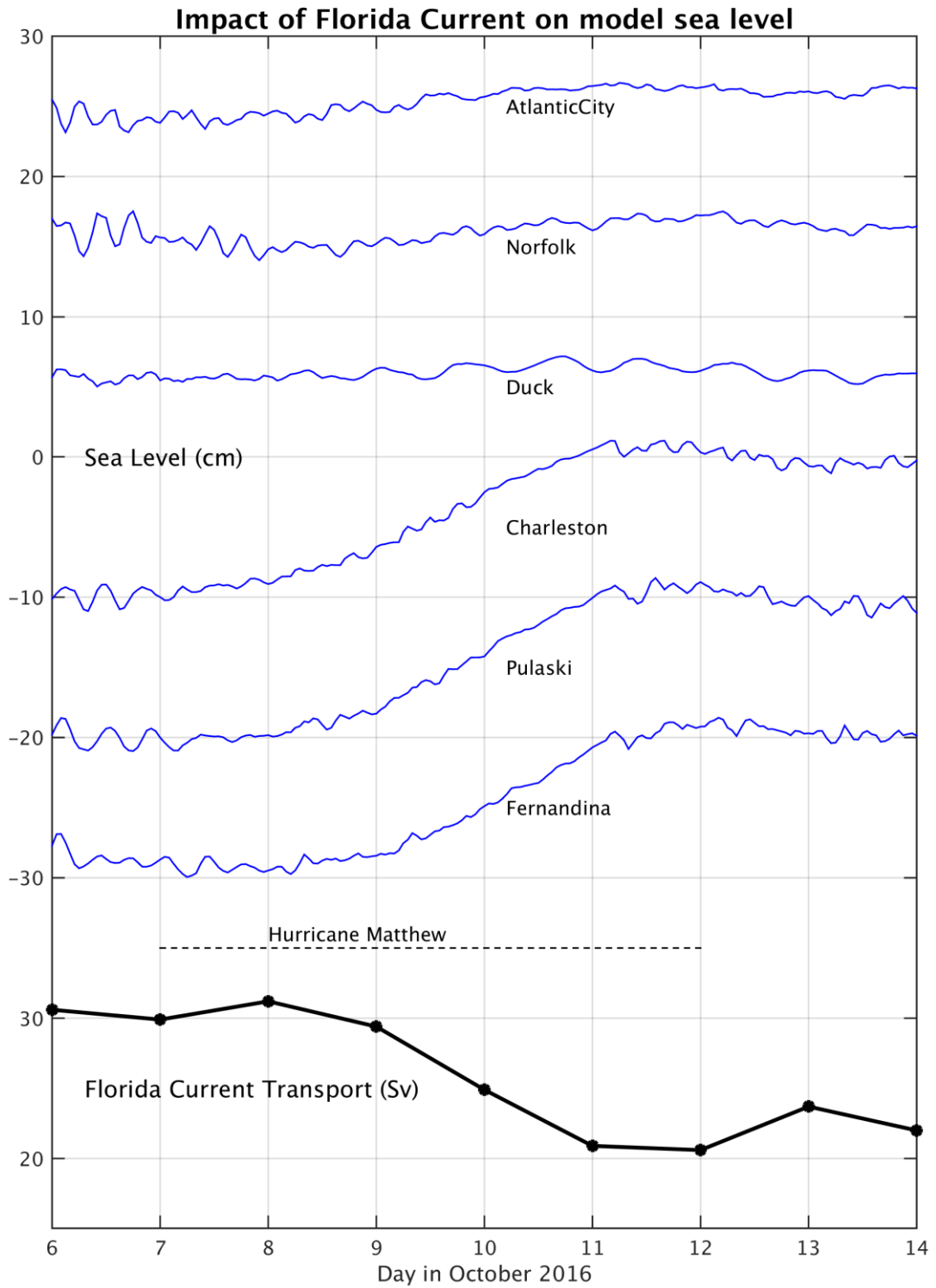
(b) Altimeter SL Anomaly 12-OCT-2016



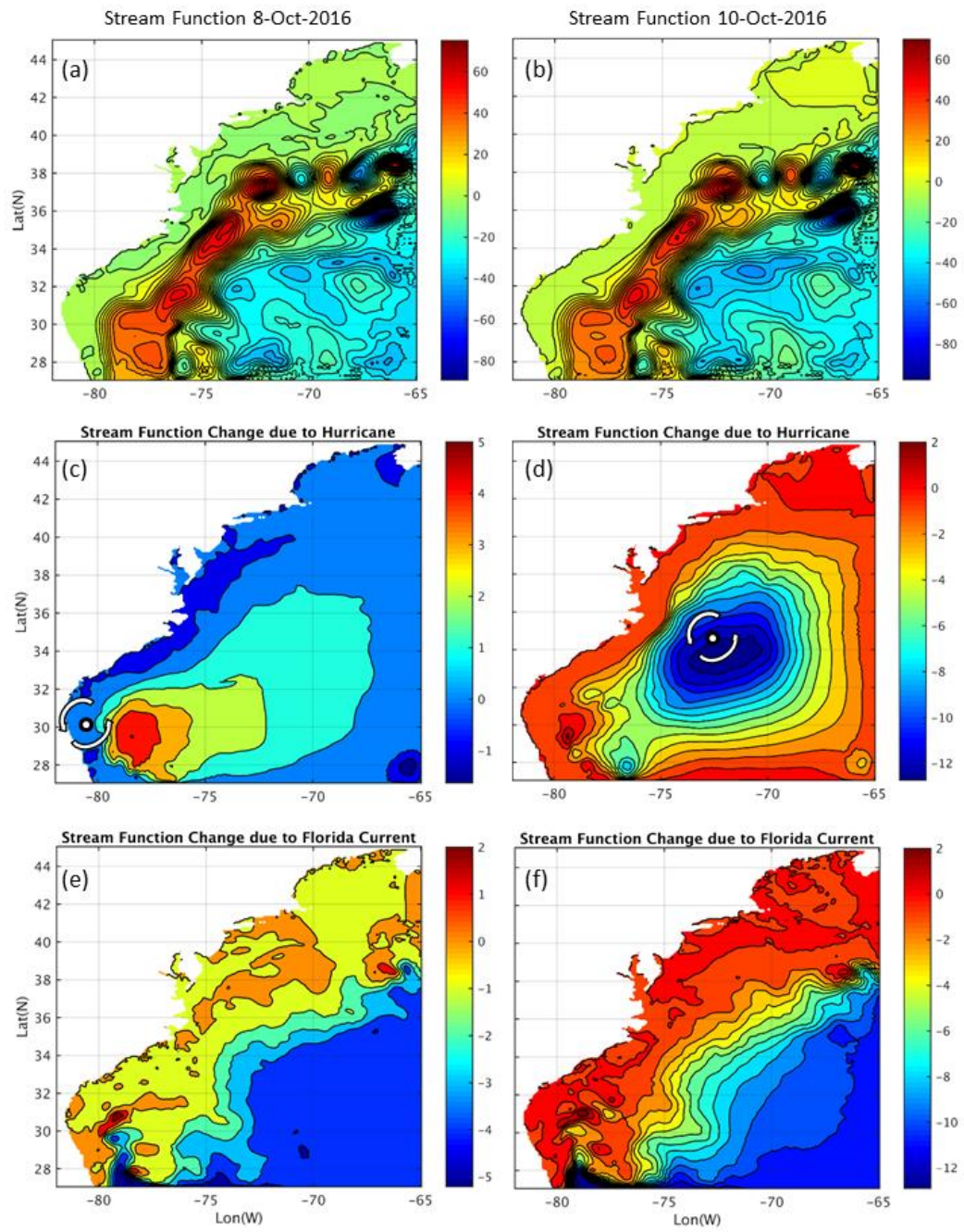
550
551 Fig. 4
552



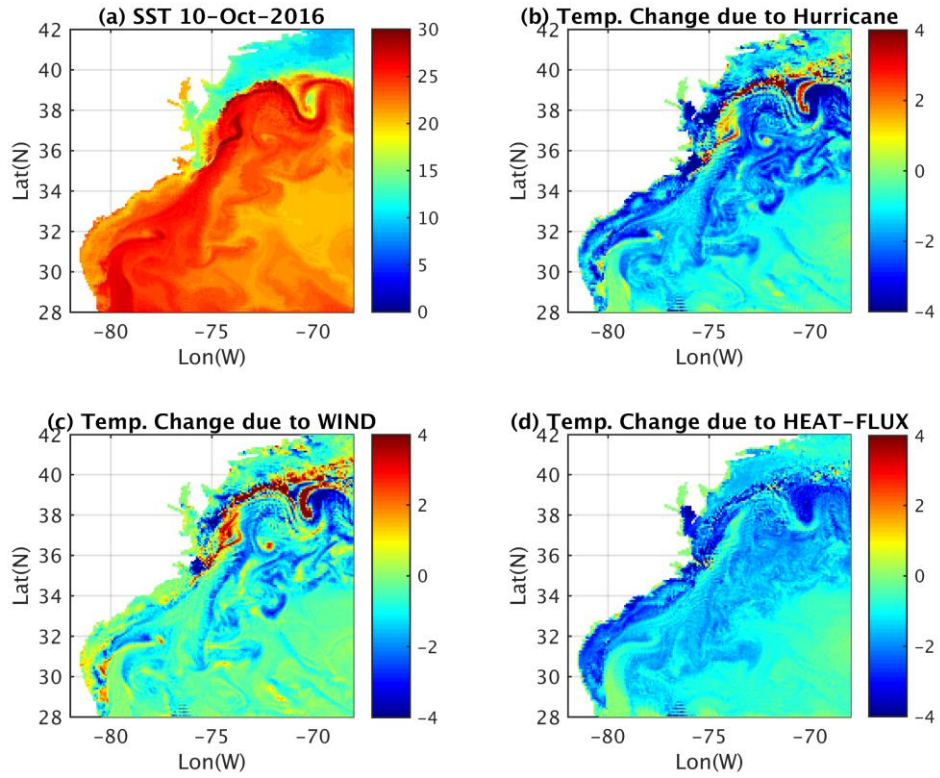
553 Fig. 5
 554
 555



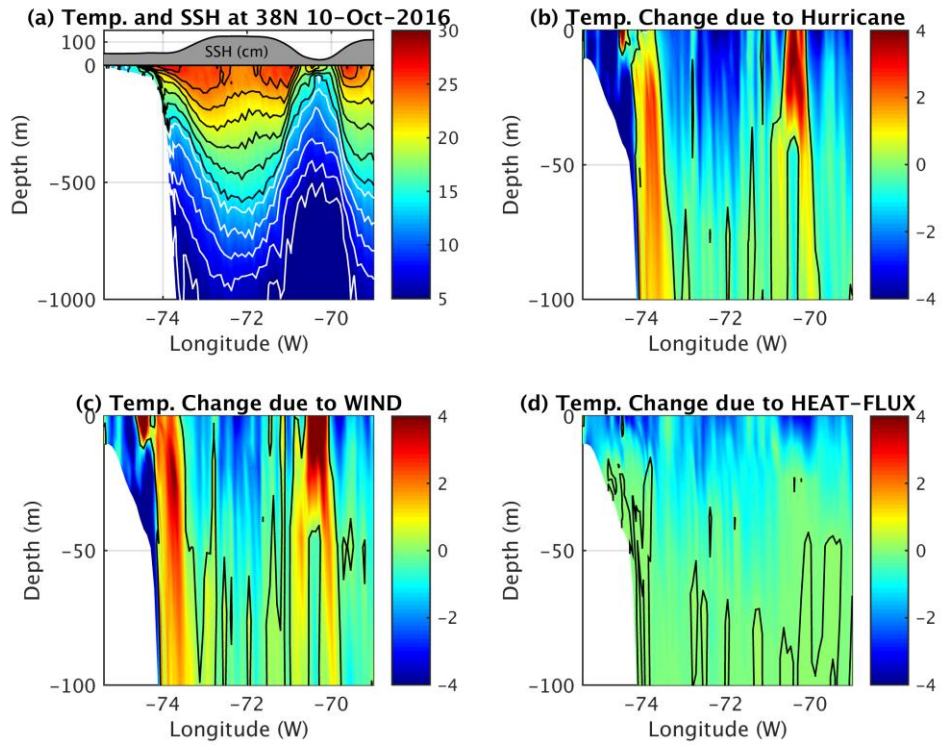
556 Fig. 6
 557
 558



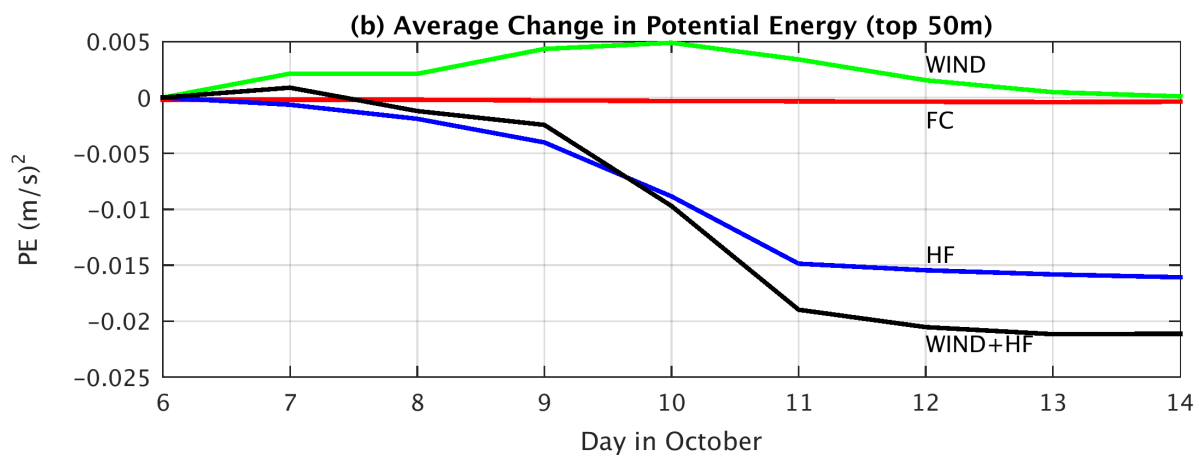
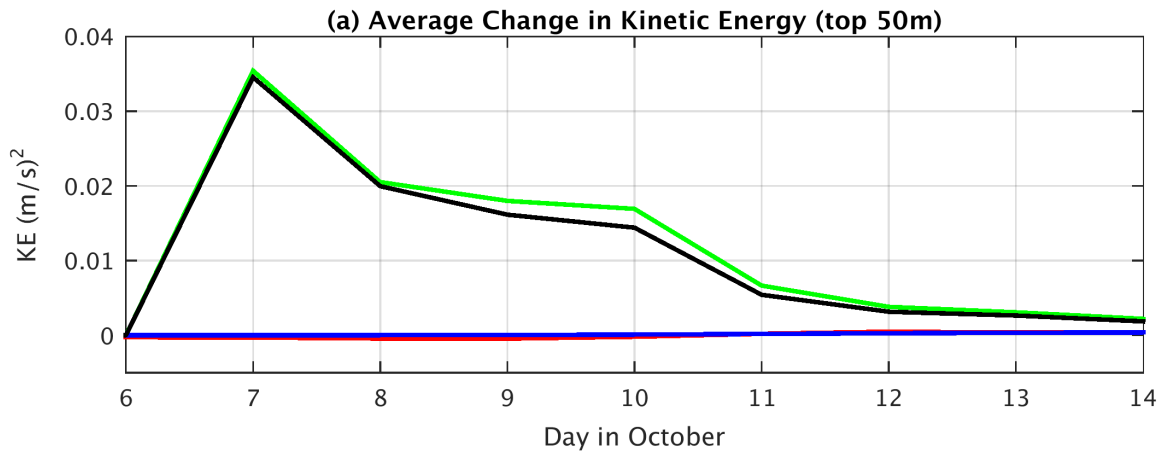
559
 560 Fig. 7
 561
 562



563
564 Fig. 8
565
566



567
568 Fig. 9
569



570
571
572 Fig. 10